4.1 Recent Progress in the Development of Ductile-Phase Toughened Tungsten for Plasma-Facing Materials — C. H. Henager, Jr., R. J. Kurtz, T. J. Roosendaal, and B. A. Borlaug (Pacific Northwest National Laboratory), G. R. Odette, K. H. Cunningham, K. Fields, D. Gragg, and F. W. Zok (University of California, Santa Barbara)

OBJECTIVE

The objective of this study is to develop the materials science of fiber-reinforced tungsten composites as candidates for plasma-facing components in future fusion reactors.

SUMMARY

Tungsten (W) and W-alloys are the leading candidates for plasma-facing components in nuclear fusion reactor designs because of their high melting point, strength at high temperatures, and low sputtering yield. However, tungsten is brittle and does not exhibit the required fracture toughness for nuclear applications. The ductile-brittle transition temperature (DBTT) for unirradiated W-alloys ranges from 300-1000ºC and radiation hardening further elevates this range. A promising approach to increasing fracture toughness and decreasing the DBTT of a W-alloy is by ductile-phase toughening (DPT). In this method, a ductile phase is included in a brittle matrix to prevent fracture propagation by crack bridging. To examine the prospect of DPT, W-Cu and W-Ni-Fe three-point bend samples were deformed at several strain rates and temperatures. Data from these tests will be used for time-dependent crack bridging studies and the calibration of a crack-bridging model that can effectively predict elevated temperature crack growth in W-composites. A study of fabricating W-wire-reinforced W-matrix composites by spark plasma sintering (SPS) was initiated. W-wires coated with Cu or tungsten carbide (WC) was consolidated in a W matrix. Characterization of these composites is ongoing.

PROGRESS AND STATUS

Background

Tungsten (W) and W-alloys are the solid materials of choice for the plasma-facing components (PFCs) of future fusion reactors, such as the International Thermonuclear Experimental Reactor (ITER) and Demonstration Power Plant (DEMO), due to their high melting point, strength at high temperatures, high thermal conductivity, low coefficient of thermal expansion, and low sputtering yield [1-5]. However, W and most W-alloys exhibit low fracture toughness and a high ductile-brittle transition temperature (DBTT) that would render them as brittle materials in reactor operations [1, 3, 6]. The DBTT for unirradiated W-alloys typically ranges from 573K to 1273K (300 to 1000˚C) and in a reactor environment radiation hardening would further elevate this range [3, 7, 8]. Metallurgical approaches to toughen W-alloys, including rhenium (Re)-alloying and severe plastic deformation (SPD), have resulted in modest DBTT decreases [7, 9]. However, they would be difficult or impossible to implement, due to high costs and implications to irradiation hardening (Re alloys) or extremely complex processing demands (SPD) [10-12]. To prevent mechanical failure, a toughening mechanism is needed for W before it can be considered an effective plasma facing component material (PFCM). W-alloys toughened by engineered reinforcement architectures, such as ductile-phase toughening (DPT), are strong candidates for PFCMs. In DPT, a ductile phase is included in a brittle matrix to prevent fracture propagation. This is accomplished by the formation of an intact bridging zone behind the crack tip, which provides reinforcement, resulting in an increase in the remote load stress intensity for

[1] PNNL is operated for the U.S. Department of Energy by Battelle Memorial Institute under Contract DE-AC06-76RLO 1830.

continued crack growth with increasing crack length [13-14]. In Figure 1a, optical evidence of the crack bridging property of DPT can be seen in a W-Cu alloy.

The principles of DPT are illustrated in Figure 1b, which shows a schematic of ductile bridging ligaments stretching across an open crack in a brittle matrix material, such as W [13-14]. For a brittle material containing a suitable volume fraction of a ductile phase, a highly effective resistance curve toughening mechanism develops as the crack extends. As the crack propagates through a brittle matrix, it leaves a bridging zone of ductile ligaments over a length $\boldsymbol{L}$ behind the crack tip. As the crack extends, $\boldsymbol{L}$ increases. For small scale bridging (SSB), when the bridging zone is much smaller than the length of the crack, $\boldsymbol{L}$ reaches a steady state ($\boldsymbol{L} = \boldsymbol{L_{SSB}}$). The ligaments act in opposition to the applied loading stress intensity factor, $\boldsymbol{K_{Applied}}$. This reduces the crack tip stress intensity factor so that: $\boldsymbol{K_{Tip}} < \boldsymbol{K_{Applied}}$. The crack opening (u) increases with increasing distance behind the crack-tip until the reinforcement breaks at a critical u*.

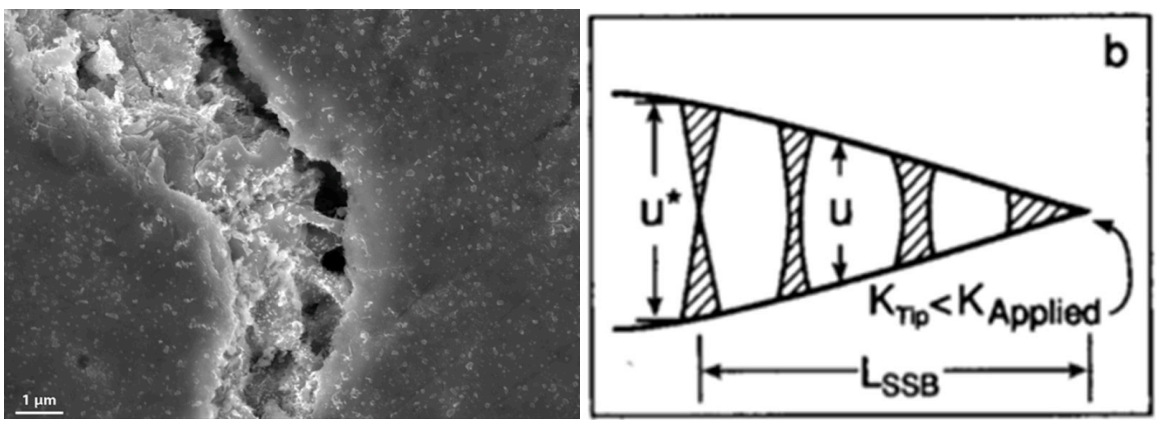

Figure 1. a) SEM image of W-Cu fracture where the ductile phase (Cu) is effectively bridging the crack. b) A steady-state bridging zone shown schematically in 2D [14].

Experimental

Elevated temperature testing of notched and pre-cracked three-point bend specimens was performed in a tube furnace at ½ T_m, ⅔ T_m, and room temperature, where Tm is the melting point of the reinforcement (ductile) phase. For W-Cu this is the melting point of Cu, whereas for the W-Ni-Fe material the melting point of the W-Ni-Fe phase was approximated from the phase diagram by the melting point of Ni. Displacement rates of 0.0002, 0.002, 0.02, 0.2, and 2.0 mm/min were employed. Purified Ar gas flowed through the tube furnace to prevent specimen oxidation. W-Cu and W-Ni-Fe alloys were evaluated using fracture mechanics test methods to gather quantitative data on the effects of DPT. Similar tests on monolithic W were performed to provide a baseline for comparison to these materials [15]. Tungsten matrix-tungsten wire-reinforced composites were fabricated by SPS. Copper was electrodeposited on the W-wires, while the WC coating was created by SPS packing W-wires in graphite powder.

The W-Cu System

The W-Cu system served as a model system for the initial exploration of DPT in W-alloys [15]. Although not a plausible choice for nuclear applications due to Cu's low melting temperature, it was chosen with the goal of maximizing the plastic $\sigma(u)$ of the Cu reinforcement. The data gathered would be used to develop a fully quantitative model of DPT in the W-Cu system that will aid in future research to develop an effective W-based PFCM. A working hypothesis for this composite material is that the fracture properties are determined by the ductile-phase mechanical properties, which in this case is the Cu phase.

The W-25% Cu (by weight) composite, Copelmet®, was purchased by UCSB and sent to PNNL in the form of 3.30mm x 1.67mm x 16.05mm bend bars for mechanical testing [15]. The bars were EDM notched to a depth (a_n) over bar width (w) ratio of a_n/w =0.2. Slight variances in specimen geometry (including notch depth) were accounted for by computing the peak-load linear elastic stress intensity factor (K_{peak}).

The W-Ni-Fe System

W-Ni-Fe testing was conducted in order to investigate the fracture behavior of another common, W-based heavy alloy. The microstructure is comprised of a continuous network of spheroidal crystals embedded in a ductile, fcc matrix phase. Such W-composites have been studied for some time [16-26] and this report will not be able to cover the entire range of chemical, compositional, and mechanical data found in the literature. Here the focus is on determining for the future if such materials can be useful for fusion reactor applications. The overall chemical composition is 85% W, 11.7% Ni, and 3.3% Fe (by weight), where the spheroidal crystals are 99.5% W, 0.3% Ni, and 0.2% Fe, and the matrix is 56.9% Ni, 29.3% W, and 13.8% Fe. An SEM image with chemical compositional data is shown in Figure 2. The overall composition is 85-wt% W with the particles 99.5% W and the matrix 29.3% W. The balance of the matrix is Ni and Fe as indicated. Electron backscatter diffraction (EBSD) data indicated that the matrix phase was single crystal and indexed as an fcc Ni-based superalloy structure. A particle areal fraction analysis indicated that an estimate of the particle volume fraction is 78.2% ± 2.3%.

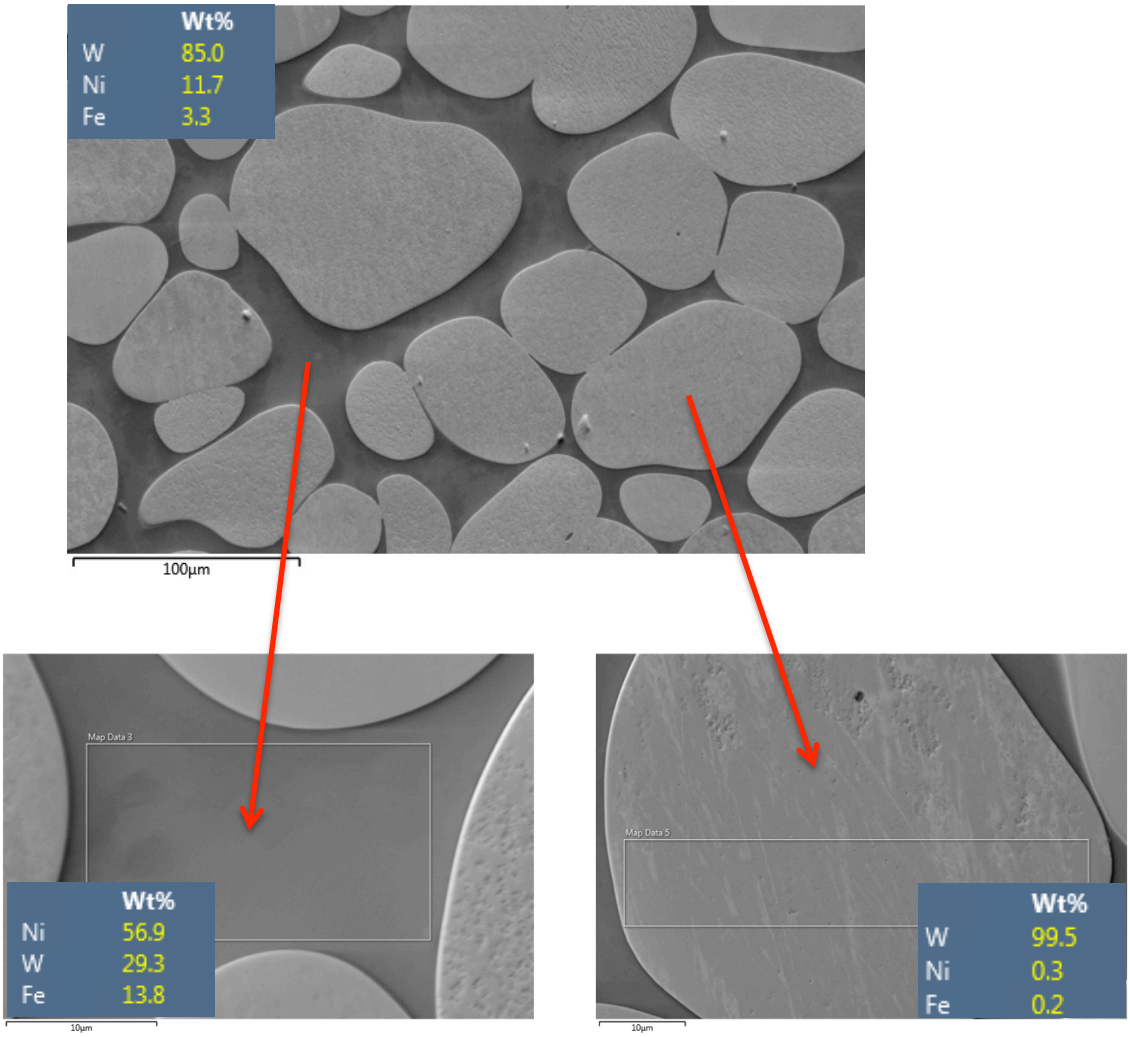

Figure 2. SEM images of a representative region of the W-Ni-Fe materials along with EDS composition results given in weight percent in the inset tables. The materials are liquid phase sintered from powders and these particular materials are archival materials from PNNL from prior research projects.

To test the mechanical properties of the W-Ni-Fe alloy, 4mm x 3mm x 20mm bend bars were fabricated and three-pint bend tests were conducted. The bars were notched to a depth (a_n) over bar width (W) ratio of a_n/W=0.25 and testing was performed over a range of temperatures and strain rates as for the W-Cu.

Three-Point Bend Testing

Testing was conducted on an Instron 5582 test frame with the following parameters: 1) Test temperatures were ambient, ½ T_M and ⅔ T_M, and 2). Strain rates were 0.0002 to 2 mm/min covering each decade. All high temperature testing was conducted in flowing purified argon (Ar) to prevent oxidation of the sample.

Peak Stress Intensity Calculation

Calculations of K_{Peak} were made from the 3-point SENB data using the peak load and equations A3.1 and A3.2 in ASTM-E399-12, "Standard Test Method for Linear-Elastic Plane-Strain Fracture Toughness KIC of Metallic Materials" [27]. At this stage of research, K_{Peak} provides an approximate toughness-based method for comparing the mechanical properties of the two W-alloys by accounting for differences in specimen and crack geometry. The results are not meant to be interpreted as fracture toughness data.

The W-W Fiber-Reinforced Composite System

The interface between the two W phases is critical to the mechanical performance of the composite. A Cu coating was investigated because of its insolubility in W. WC was investigated as a potential debonding layer. Copper coatings up to 25 μm thick were electrodeposited on W wires; Twelve mm lengths of coated wire were placed in W powder in a die perpendicular to the pressing direction and subjected to SPS in the same manner as previous pure W samples (see row 1 in Table 1). Results from the first trial prompted the investigation of a different SPS route (see row 2 in Table 1) using two dwell temperatures. The intent was to consolidate the W sufficiently in the vicinity of the coated wire below the melting point of Cu, so that it would be localized at the wire-matrix interface prior to a high-temperature dwell to fully consolidate the matrix. The consolidated samples were examined using SEM and EBSD.

To carburize the W wire, 12 mm lengths of W-wire were cut and laid separately in a bed of graphite powder (2-15 μm particle size, Alfa Aesar), then pressed and heated using the SPS system (see row 3 in Table 1). Coated wires were cleaned in an ultrasonic bath to remove excess graphite particles, and then laid in W powder in the same manner above and consolidated via SPS (see row 4 in Table 1).

Table 1. Summary of process parameters for SPS system and outcomes for composite fabrication and W-wire carburization.

Materials	Pressing	Heating rate	Dwell T	Dwell t	Result
Cu-coated W wire + W	50 MPa	100 C/min	1700 C	5 min	Cu melted, found in matrix pores
Cu-coated W wire + W (2-T route)	50 50	100 100	990 1700	25 0	Cu melted, found in matrix pores
W wire + C	35 before heating, 9.5 during heating	300	1800	1	WC coating on wire ~12 μm
WC-coated W wire + W	50	100	1900	10	WC intact at interface

RESULTS

W-Cu

At room temperature, the peak stress intensity of W-Cu (≈20-24 MPa√m) is approximately three times greater than that of monolithic W (≈8 MPa√m) [15]. Figure 3 shows the effects of temperature and deformation rate on the peak stress intensity of W-Cu.

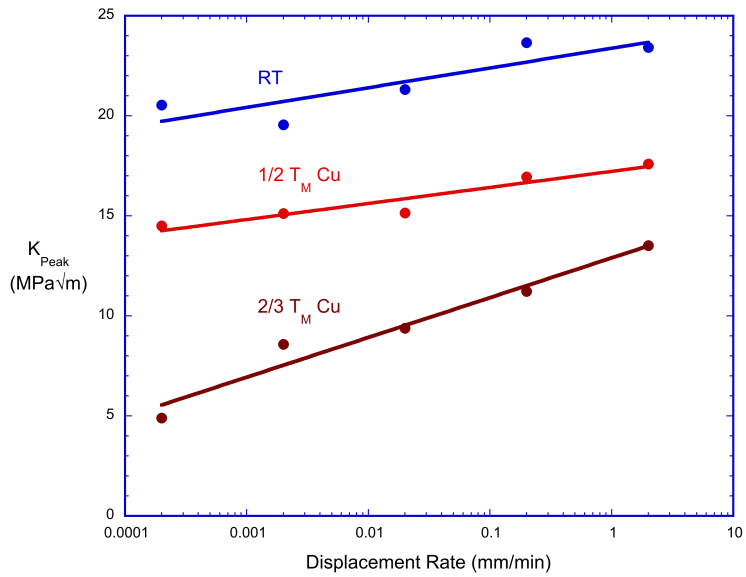

Figure 3. Dependence of peak stress intensity of the W-Cu composite on deformation rate and test temperature.

W-Ni-Fe

At room temperature, the peak stress intensity of the W-Ni-Fe composite (≈32-58 MPa√m depending on deformation rate) is approximately four to eight times greater than that of monolithic tungsten, and two to three times greater than that of the W-Cu. Figure 4 shows the effect of deformation rate on the peak stress intensity of W-Ni-Fe at room temperature.

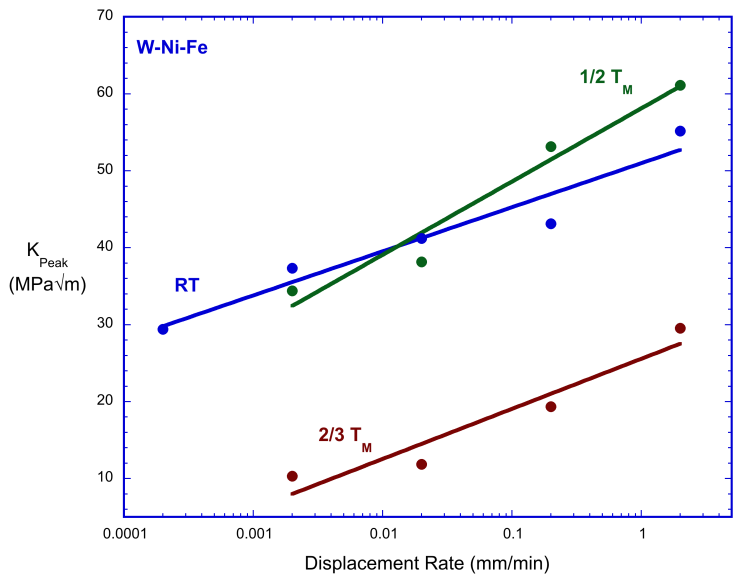

Figure 4. Dependence of peak stress intensity of the W-Ni-Fe composite on deformation rate and test temperature.

A graphical comparison of the W-Cu and W-Ni-Fe data at ambient temperature as a function of strain rate is shown in Figure 5. The W-Ni-Fe material is clearly much stronger and tougher but does have a much higher strain rate dependence compared to the W-Cu composite.

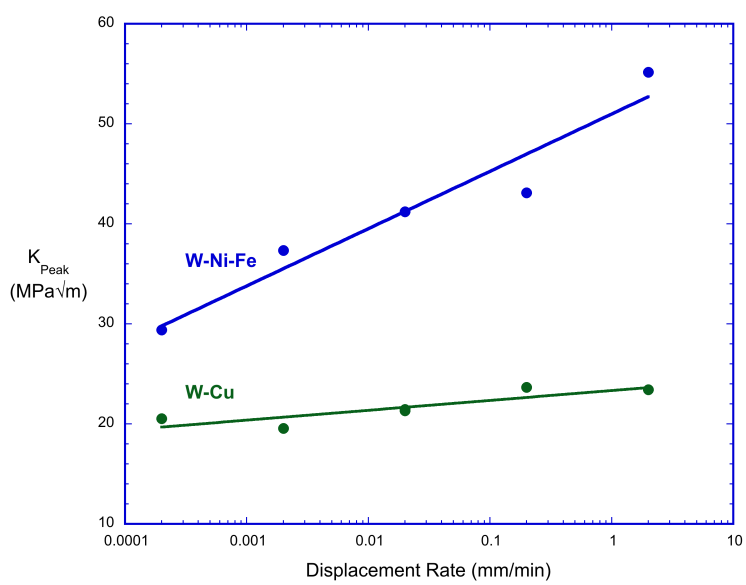

Figure 5. A comparison plot of peak load stress intensity as a function of displacement rate for W-Cu and W-Ni-Fe composites at ambient temperature.

W-W Fiber-Reinforced Composite

In the case of the Cu coated wires, neither sintering method successfully maintained a Cu layer at the wire-matrix interface; rather, a small amount of wicked Cu was found to coat the walls of the matrix W-powder pores (see Figure 6). Notably, the wires maintained a fine grain size of 0.3-3 μm with a <110> axial texture after processing (see Figure 7). In contrast, the 12-μm WC coating was intact after consolidation. Characterization of the WC-coated wire composite is ongoing.

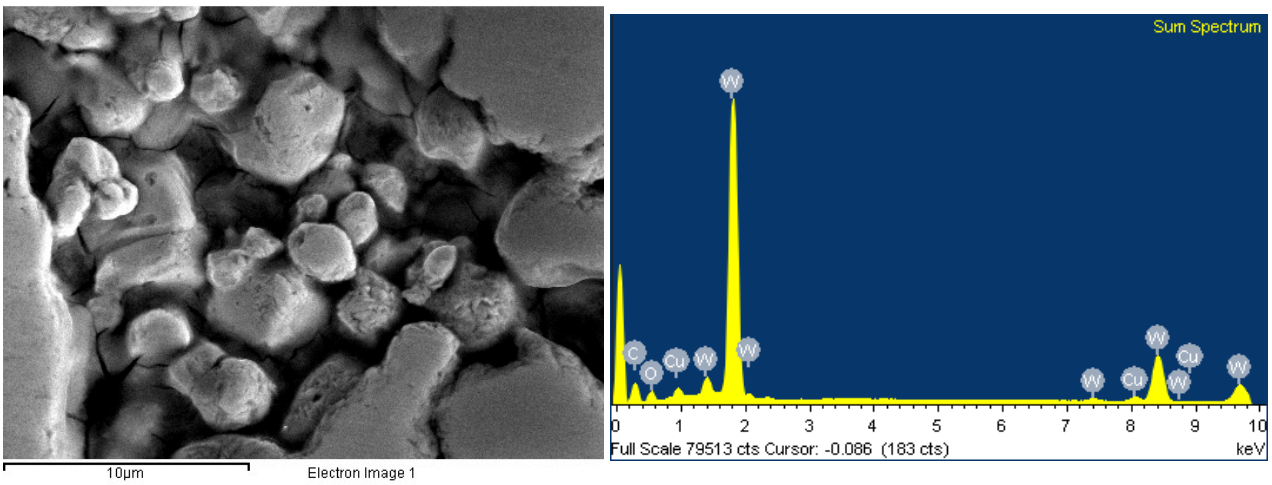

Figure 6. SEM image of a porous area in W matrix, scale bar 10 μm. Sample is single-temperature SPS route for W powder consolidated around Cu-coated W wires. EDS spectrum shows Cu detected in pore. Cu was not found at the wire-matrix interface.

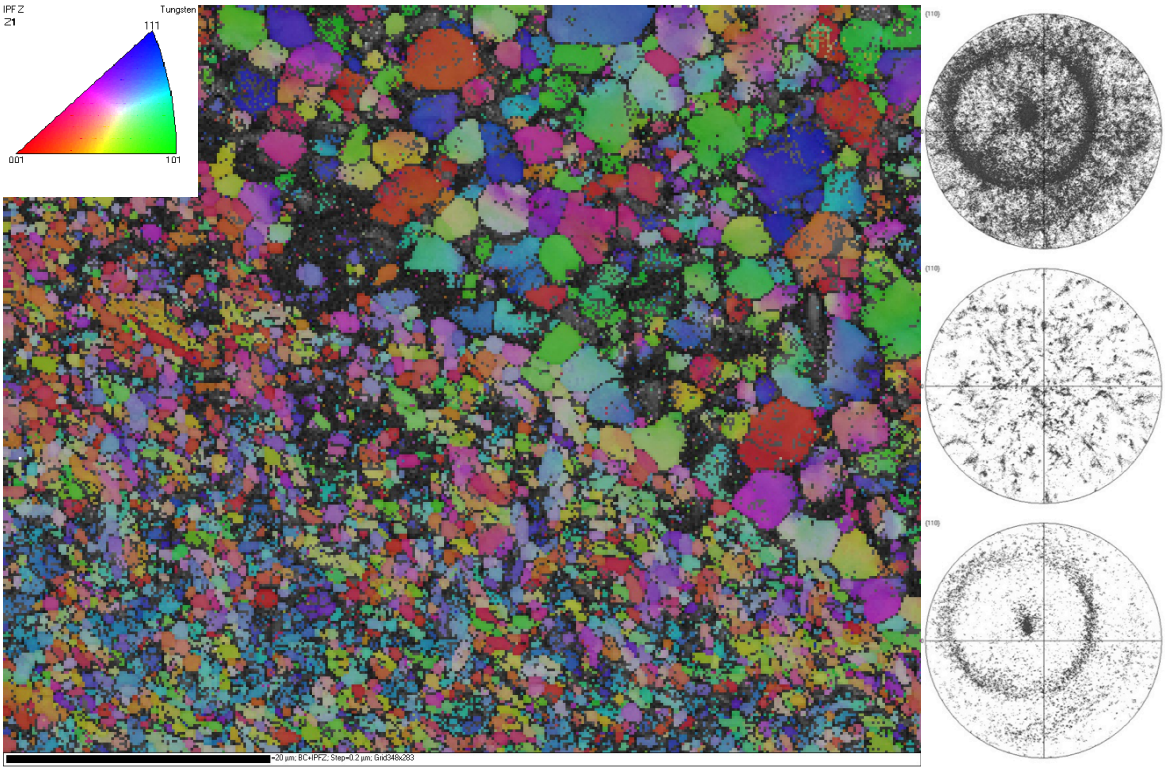

Figure 7. EBSD pole figures and band contrast images of the W wire adjoining showing strong <110>-texturing and fine grain sizes in the Fe. From top to bottom the pole figures are 1) full frame, 2) matrix only, 3) wire only.

FUTURE WORK

In the immediate future, testing on the W-Ni-Fe system will be concluded. A bridging model will be constructed for the W-Cu alloys and it is not apparent that such a model is suitable for the W-Ni-Fe alloys yet. The model, along with fracture data, the method and cost of synthesis, and microstructure examinations will be used to guide the future design of improved W-composites. Further characterization and mechanical testing of the W-W fiber-reinforced composites will be performed. Additional fabrication routes will be investigated, including foil-wire diffusion bonding and accumulative roll bonding. Ultimately, a clear understanding of the materials science of W-composites should be developed with relation to: a) the choice and behavior of the ductile phase; b) the synthesis, processing, and fabrication of composites; and c) the composite's microstructure as it evolves during service.

REFERENCES

[1] M. Rieth, J. L. Boutard, S. L. Dudarev, et al., "Review on the EFDA programme on tungsten materials technology and science," *J. Nucl. Mater.* **417**, 463-467 (2011).

[2] R. A. Pitts, A. Kukushkin, A. Loarte, A. Martin, M. Merola, C. E. Kessel, V. Komarov, and M. Shimada, "Status and physics basis of the ITER divertor," *Phys. Scr.* **Volume T, 22009(T138)**, 014001.

[3] P. Mertens, T. Hirai, M. Knaup, O. Neubauer, V. Philipps, J. Rapp, V. Riccardo, S. Sadakov, B. Schweer, A. Terra, I. Uytdenhouwen, and U. Samm, "A bulk tungsten divertor row for the outer strike point in JET," *Fusion Eng. Des.* **84(7-11)**, 1289-93 (2009).
[4] A. Gervash, R. Giniyatulin, T. Ihli, W. Krauss, A. Makhankov, I. Mazul, P. Norajitra, and N. Yablokov, "Fabrication of a He-cooled divertor module for DEMO reactor," *J. Nucl. Mater.* **367-370** B(SPEC. ISS.), 1472-1475 (2007).
[5] M. Merola, W. Danner, and M. Pick, "EU RD on divertor components," Fusion Eng. Des. **75-79**(SUPPL.), 325-331 (2005).
[6] P. Mertens, V. Philipps, G. Pintsuk, V. Riccardo, U. Samm, V. Thompson, and I. Uytdenhouwen, "Clamping of solid tungsten components for the bulk W divertor row in JET-precautionary design for a brittle material," Phys. Scr. **Volume T, 2009(T138)**, 014032.
[7] B. Gludovatz, S. Wurster, A. Hoffmann, and R. Pippan, "Fracture toughness of polycrystalline tungsten alloys," *Int. J. Refract. Metals Hard Mater.* **28**(6), 674-8 (2010).
[8] S. J. Zinkle, and N. M. Ghoniem, "Operating temperature windows for fusion reactor structural materials," *Fusion Eng. Des.* **51-52**, 55-71 (2000).
[9] M. Faleschini, H. Kreuzer, D. Kiener, and R. Pippan, "Fracture toughness investigations of tungsten alloys and SPD tungsten alloys," *J. Nucl. Mater.* **367-370** A(SPEC. ISS.), 800-805 (2007).
[10] T. Tanno, A. Hasegawa, J. C. He, M. Fujiwara, M. Satou, S. Nogami, K. Abe, and T. Shishido, "Effects of transmutation elements on the microstructural evolution and electrical resistivity of neutron-irradiated tungsten," *J. Nucl. Mater.* **386-388(C)**, 218-221 (2009).
[11] T. Tanno, A. Hasegawa, M. Fujiwara, H. Jian-Chao, S. Nogami, M. Satou, T. Shishido, and K. Abe, "Precipitation of solid transmutation elements in irradiated tungsten alloys," *Mater. Trans.* **49**(10), 2259-64 (2008).
[12] T. Tanno, A. Hasegawa, H. Jian-Chao, M. Fujiwara, S. Nogami, M. Satou, T. Shishido, and K. Abe, "Effects of transmutation elements on neutron irradiation hardening of tungsten," *Mater. Trans.* **48**(9), 2399-402 (2007).
[13] R. Venkateswara, G. R. Odette, and R. O. Ritchie, "Ductile-reinforcement toughening in -TiAl intermetallic-matrix composites: effects on fracture toughness and fatigue-crack propagation resistance," *Acta Metall. Mater.* **42**(3), 893-911 (1994).
[14] G. R. Odette, B. L. Chao, J. W. Sheckherd, and G. E. Lucas, "Ductile phase toughening mechanisms in a TiAl-TiNb laminate composite," *Acta Metall. Mater.* **40**(9), 2381-9 (1992).
[15] K. H. Cunningham, K. Fields, D. Gragg, F. W. Zok, J. C. H. Henager, R. J. Kurtz, and T. Roosendaal, Recent Progress in the Development of Ductile-Phase Toughened Tungsten for Plasma-Facing Materials, in DOE/ER-0313/54 - Volume 54, Semiannual Progress Report, June 30, 2013. 2013, US DOE: ORNL, TN.
[16] N. Durlu, N. K. Caliskan, and S. Bor, "Effect of swaging on microstructure and tensile properties of W-Ni-Fe alloys," *Int. J. Refract. Metals Hard Mater.* **42**, 126-131 (2014).
[17] J. Zhu, S. Cao, and H. Liu, "Fabrication of W-Ni-Fe alloys with gradient structures," *Int. J. Refract. Metals Hard Mater.* **36** 72-75 (2013).
[18] R. Muresan, E. Riti-Mihoc, C. Prica, and M. Bodea, "Improving mechanical properties of sintered wolfram based alloy with liquid phase trough controlled cooling parameters," *Arch. Metall. Mater.* **57**(1), 87-92 (2012).
[19] J. Das, U. R. Kiran, A. Chakraborty, and N. E. Prasad, "Hardness and tensile properties of tungsten based heavy alloys prepared by liquid phase sintering technique," *Int. J. Refract. Metals Hard Mater.* **27**(3), 577-583 (2009).

[20] K. H. Lee, S. I. Cha, H. J. Ryu, and S. H. Hong, "Effect of two-stage sintering process on microstructure and mechanical properties of ODS tungsten heavy alloy," *Mater. Sci. Eng. A,* **458**(1-2), 323-329 (2007).
[21] L. Woei-Shyan, L. Chi-Feng, and C. Sen-Tay, "Plastic flow of tungsten-based composite under hot compression," *J. Mater. Process. Technol.* **100**(1-3), 123-30 (2000).
[22] Y. H. Chiou, Y. S. Zu, and S. T. Lin, "Partition of tungsten in the matrix phase for liquid phase sintered 93%W-4.9%Ni-2.1%Fe," *Scr. Mater.* **34**(1), 135-40 (1996).
[23] R. S. Coates, and K. T. Ramesh, "Rate-dependent deformation of a tungsten heavy alloy," *Mater. Sci. Eng. A* **145(**2), 159-166 (1991).
[24] A. Bose, D. Sims, and R. M. German, "Test temperature and strain rate effects on the properties of a tungsten heavy alloy," *Metall. Trans. A (Phys. Metall. Mater. Sci.)* **19A**(3), 487-94 (1988).
[25] K. S. Churn and R. M. German, "Fracture behavior of W-Ni-Fe heavy alloys," *Metall. Trans. Phys. Metall. Mater. Sci.)* **15A**(2), 331-8 (1984).
[26] E. G. Zukas, E. G. and H. Sheinberg, "Sintering mechanisms in the 95% W-3.5% Ni-1.5% Fe composite," *Powder Technol.* **13**(1), 85-96 (1976).
[27] ASTM, Standard Test Method for Linear-Elastic Plane-Strain Fracture Toughness KIC of Metallic Materials, in E399-12, 2012, ASTM International: West Conshohocken, PA.